Applied Clay Science 80–81 (2013) 398–406

Contents lists available at ScienceDirect

Applied Clay Science

journal homepage: www.elsevier.com/locate/clay

Research paper

Thermal degradation of organic matter in the interlayer clay–organic complex: A TG-FTIR study on a montmorillonite/12-aminolauric acid system

Hongmei Liu [a], Peng Yuan [a,*], Zonghua Qin [c], Dong Liu [a], Daoyong Tan [a,b], Jianxi Zhu [a,b], Hongping He [a]

[a] CAS Key Laboratory of Mineralogy and Metallogeny, Guangzhou Institute of Geochemistry, Chinese Academy of Sciences, Guangzhou 510640, China
[b] University of Chinese Academy of Sciences, Beijing 100049, China
[c] State Key Laboratory of Ore Deposit Geochemistry, Institute of Geochemistry, Chinese Academy of Sciences, Guiyang 550002, China

ARTICLE INFO

Article history:
Received 23 October 2012
Received in revised form 28 April 2013
Accepted 14 July 2013
Available online 15 August 2013

Keywords:
Interlayer clay–organic complex
Thermal degradation
TG-FTIR
Solid acidity

ABSTRACT

The storage of natural organic matter within the interlayer space of layered silicate is an important type of clay–organic association in sediment. However, the role of the interlayer space of clay minerals in the thermal degradation of organics and the generation of hydrocarbons has not been well understood. In this study, an interlayer clay–organic complex was synthesized using montmorillonite (Mt) and 12-aminolauric acid (ALA). An Mt–ALA complex in which Mt and ALA were simply mixed was also prepared for comparison. Thermogravimetry coupled with Fourier transform infrared spectroscopy (TG-FTIR) was applied to monitor the thermal events and the corresponding products during the thermal degradation of the Mt–ALA complexes. In the absence of Mt, ALA decomposed at 467 °C via the cleavage of C–C bonds, producing aliphatic hydrocarbon, N-containing compounds, and carboxylic acid. The decomposition temperatures of organic matter in the mixed Mt–ALA complex and the interlayer Mt–ALA complex decreased to 402 and 342 °C, respectively. The most characteristic products of the interlayer Mt–ALA complex were NH_3 and saturated hydrocarbons. The Brønsted acid sites in the interlayer space of Mt, arising from the dissociated interlayer water, initiated the deamination of ALA via the Hoffmann elimination pathway and significantly promoted the cracking of hydrocarbons via a carbonation mechanism. Lewis acid sites had little effect on the thermal degradation of ALA. This work indicated that the interlayer space of clay minerals provided the storage space for organic matter. Moreover, the active sites within the interlayer space strongly promoted the thermal degradation of organics.

1. Introduction

Clay mineral catalysis has been generally accepted to be an important factor in the transformation of organic matter into gas and oil (Geatches et al., 2010; Johns, 1979; Wei et al., 2006). Numerous studies have demonstrated that clay minerals affect the amount, composition, and distribution of the pyrolysis products of natural or pure organics (Heller-Kallai et al., 1984; Jurg and Eisma, 1964; Pan et al., 2010; Shimoyama and Johns, 1971; Tannenbaum and Kaplan, 1985). However, clay-induced catalytic reactions still need to be further understood because of the complexity of the components of natural organics and the complicated association between organics and clay minerals.

Organic matter in sediment is primarily associated with clay minerals as a result of several processes, including adsorption, bounding, and intercalation (Wattel-Koekkoek et al., 2001). The storage of organic matter within the interlayer space of layered silicates, which is an important type of clay–organic association in soil, has been proposed and confirmed by previous studies (Lagaly et al., 2006; Theng, 1974; Theng et al., 1986). Cai et al. (2007) analyzed the organic matter in clay fraction of muddy sediment and mudstone using X-ray diffraction (XRD) and differential thermal analysis (DTA) technique. They found that the clay mineral interlayer space of XRD curves and exothermic peaks of DTA curves both changed as heating temperature increased. The change of clay mineral interlayer space and exothermic peaks were concordant and stable around 350 °C, indicating that organic matter entered clay mineral interlayers to form stable clay–organic complexes. These interlayer clay–organic complexes have also been observed in some source rocks. Lu et al. (1999) investigated the combination of soluble organic matters and clay minerals in source rock and found that the interlayer distances of the clay minerals had decreased significantly after the associated organic matter was extracted, which strongly proved the existence of natural organics in the interlayer space. The content of the interlayer organics accounted for approximately 25–50 wt.% of the total extracted organics, which indicates the significance of the interlayer organics in resource assessments. Kennedy et al. (2002) also found that organic matter was sequestered within the interlayer space of smectite clay in Cretaceous black shale. Moreover, experimental study indicated that some organic constituents, who are of importance in petroleum generation, can enter into

* Corresponding author. Tel./fax: +86 20 85290341.
E-mail address: yuanpeng@gig.ac.cn (P. Yuan).

0169-1317/$ – see front matter © 2013 Elsevier B.V. All rights reserved.
http://dx.doi.org/10.1016/j.clay.2013.07.005

the interlayer space of clay minerals. Wang and Huang (1986) reported that, hydroquinone, a precursor for the formation of humic substances (precursor of kerogen), was able to transform in aqueous solution even at near-neutral pH (6.5) to humic macromolecules and adsorbed in the interlayer of smectite. Cosultchi et al. (2004) found that both paraffin and aromatic type molecules (n-heptane and toluene) used in the experiments were able to occupy the clay interlayer space when separately contacted with clay. Moreover, the compounds containing alkane chains in crude oil preferentially diffused within the clay interlayer and occupied the interlayer space. However, to the best of our knowledge, the effect of organics within the interlayer space of clay minerals on hydrocarbon generation is rarely considered.

Pure organic compounds with relatively simple structures, such as fatty acids, have been used as model compounds to simulate naturally occurring parent organics, which have highly complex compositions and structures that are difficult to analyze. The model compounds have been mixed with clay minerals, such as montmorillonite, illite, and kaolinite, to investigate the thermal degradation of organics and hydrocarbon generation in the clay–organic complex (Aizenshtat et al., 1984; Faure et al., 2006; Johns, 1979; Shimoyama and Johns, 1971; Zhang et al., 2008). However, several reports pointed out that the intercalation of those compounds into the abovementioned clay minerals cannot occur under the applied conditions (Bayrak, 2006; Drouin et al., 2010). Therefore, it is meaningful to investigate the thermal degradation of organic matters within the interlayer space of clay minerals.

Various techniques have been applied to analyze the products yielded from the thermal degradation of organics, such as gas chromatography and mass spectrometry (Mango, 2000; Pan et al., 2010; Wei et al., 2006), which provide compositional and structural information of the end products of thermal degradation. However, these techniques do not provide information about the intermediate products, which is vital for identifying the reaction sequences and understanding the related reaction mechanisms. Thermogravimetry coupled with Fourier transform infrared spectroscopy (TG-FTIR) is an effective on-line technique to continuously monitor the mass loss of samples during heating and simultaneously capture the compositional information of the corresponding gaseous products. TG-FTIR has been widely used to investigate the pyrolysis characteristics of coal (Catrinescu et al., 2006), biomass (Giuntoli et al., 2009), and polymers (Cervantes-Uc et al., 2009).

In this work, to investigate the role of the interlayer space of clay minerals in thermal decomposition of organics, an interlayer complex of montmorillonite (Mt) and 12-aminolauric acid ($NH_2(CH_2)_{11}COOH$, shortened as ALA) was prepared and used for the TG-FTIR study. A mixed Mt–ALA complex was also prepared for comparison. Mt was selected for its well-known importance in geocatalysis and for its interlayer space. ALA was used as the model organic for the following reasons. First, it contains amino and carboxyl groups and alkyl chains with moderate numbers of carbon atoms. These groups are common in natural organics (Wattel-Koekkoek et al., 2001), such as amino acids and fatty acids. Amino acids are able to transform into macromolecule by condensation polymerization, and become the precursor of oil and gas. In addition, previous study showed that amino acid may produce hydrocarbons during early diagenesis stage, contributing to the formation of Bio-thermocatalytic Transition Zone Gases (Shi et al., 1995). The decarboxylation of fatty acid and subsequent cracking are proposed to be important for petroleum generation (Jurg and Eisma, 1964; Shimoyama and Johns, 1971). Therefore, ALA is suitable for being used as a model in simulation experiments. Second, the $-NH_2$ of ALA is readily transformed to a protonated amino group ($-NH_3^+$) in acidic solution, and it can therefore be intercalated into the Mt interlayer via cation exchange to prepare the interlayer complex. Several structural and compositional analysis methods, including X-ray diffraction (XRD), elemental analysis, and infrared spectroscopy were used to characterize the Mt–ALA complexes.

2. Experimental

2.1. Materials

ALA was supplied by Tokyo Chemical Industry Co., Ltd (98%) and used without further purification. Montmorillonite (Mt) was obtained from Inner Mongolia, China. The raw sample was purified by repeated sedimentation method to remove the impurities, and the <2 μm fraction was collected and used for further experiments. The structural formula of Mt as determined from chemical analysis was: $Ca_{0.168}Na_{0.025}K_{0.013}[Si_{3.984}Al_{0.016}][Al_{1.352}Fe_{0.271}Mg_{0.365}Ti_{0.010}]O_{10}(OH)_2 \cdot nH_2O$. The cationic exchange capacity (CEC) of Mt is 110.5 mmol/100 g. Na^+-exchanged Mt was prepared by dispersing Mt in deionized water and treating with 0.5 M sodium chloride solution under vigorously stirring at 80 °C for 24 h. The solid phase was then separated from the solution and treated with fresh salt solution followed by two repetitions of the cation-exchange procedure for complete exchange. The product was repeatedly washed with distilled water and then dried at 60 °C before being ground to a powder. The sample was denoted as Na-Mt.

2.2. Preparation of Mt–ALA complexes

The preparation of interlayer Mt–ALA complex was performed according to the following procedure: 22.1 mmol ALA was added to 200 mL of 0.14 M HCl solution which was kept at 80 °C water bath. The resulting solution was added into a dispersion composing of 10 g Na-Mt and 1000 mL distilled water. The mixture was stirred at 80 °C for 30 min. The solid in the mixture was filtered and repeatedly washed with large amounts of hot distilled water, and then dried and ground to powder. The product was labeled as ALA_{inter}–Mt(Na). The simply mixed Mt–ALA complex was prepared according to the following steps. A total of 10 g of Mt sample and 2.5 g of ALA were mixed and ground by ball milling for 20 min using a Pulverisette-6 Planetary Mill. The product was denoted as ALA–Mt(Na).

2.3. Characterization

The X-ray diffraction (XRD) patterns of the samples were recorded on a Bruker D8 Advance diffractometer with Ni filter and CuKα radiation ($\lambda = 0.154$ nm) using a generator voltage of 40 kV and a generator current of 40 mA. The scan rate was 3° (2θ)/min.

The organic content of the interlayer Mt–ALA complex was determined by elemental analysis, which was performed using an Elementar Vario EL III Universal CHNOS elemental analyzer.

The solid acidity was measured following the methods previously described (Liu et al., 2011). The total amount of solid acid sites of Na-Mt was determined by n-butylamine titration using Hammett indicators. The types of solid acid sites were differentiated by diffuse reflectance Fourier transform infrared spectroscopy using pyridine (shortened as Py) as a probe molecule. The characteristic vibrations at approximately 1540 and 1445 cm^{-1} in the FTIR spectra were attributed to the PyH^+ (Brønsted acid-bound pyridinium cation) and the coordinated Py (Lewis acid-bound Py), respectively. The amounts of Brønsted acid sites and Lewis acid sites were also calculated using the method mentioned by Liu et al.

Fourier transform infrared (FTIR) spectra of samples in pressed KBr pellets were recorded on a Bruker Vertex-70 FTIR spectrometer. The spectra were collected over the range of 600–4000 cm^{-1} with 64 scans and at a resolution of 4 cm^{-1}.

The TG-FTIR analysis was conducted on a NETZSCH STA 449C thermal analyzer coupled with a Bruker Vertex-70 Fourier-transform infrared spectrometer. Approximately 10 mg of sample was heated from room temperature to 900 °C at a rate of 20 °C/min in an ultrahigh purity argon flow (40 cm^3/min). After the evolved gases of samples from TG passing through the FTIR cell, absorbance information was obtained at

different wavenumber as a function of temperature. The FTIR spectrometer recorded spectra every 13.6 s.

3. Results and discussion

3.1. Characterization of Mt and Mt–ALA complex

The XRD patterns of ALA, Na-Mt, ALA–Mt(Na), and ALA_{inter}–Mt(Na) are displayed in Fig. 1. The basal spacing of Na-Mt is 1.22 nm (Fig. 1a). No change is observed in the (001) reflection of ALA–Mt(Na) compared with Na-Mt, which indicates that intercalation did not occur during sample preparation. The reflections with the *d*-spacings of 0.39 and 0.38 nm are assigned to the ALA planes (inset of Fig. 1). The basal spacing of ALA_{inter}–Mt(Na) is 1.70 nm, which indicates a successful intercalation of ALA into the interlayer space of Na-Mt (Fig. 1c). This result is consistent with previous reports on Mt intercalated with ALA (Ma et al., 2003; Reichert et al., 1998). As described by Reichert et al., protonated ALA entered the interlayer space of Na-Mt by cation exchange. The (002) and (003) diffractions with *d*-spacings of approximately 0.87 and 0.57 nm, respectively, are also clearly observed for ALA_{inter}–Mt(Na), which suggests that the intercalation of ALA occurs without destruction of the layered structure of Na-Mt.

The content of intercalated ALA in ALA_{inter}–Mt(Na) is 19.0 wt.%, which is calculated by the percentages of N (wt%) derived from the elemental analysis. This result is comparable to the 20.0 wt.% ALA content in ALA–Mt(Na). The intercalated amount of ALA in ALA_{inter}–Mt(Na) is 0.88 mmol/g, which is lower than the CEC value (1.11 mmol/g) of Na-Mt. This result indicates that a small quantity of Na^+ may remain in the interlayer space of ALA_{inter}–Mt(Na).

The FTIR spectra of the Na-Mt, ALA, and Mt–ALA complexes are shown in Fig. 2. The assignments of each vibration (Table 1) are based on previous reports of Mt and ALA (Katti et al., 2006; Sikdar et al., 2008). The FTIR spectrum of ALA–Mt(Na) exhibited features that are a combination of characteristic bands of Na-Mt and pure ALA (Fig. 2a and d). This result indicates that the original materials are not influenced by simple mixing, which coincides well with the XRD data.

Several differences exist between the spectra of ALA (Fig. 2c) and ALA_{inter}–Mt(Na) (Fig. 2d). The N–H stretching band of $-NH_2$ at 3187 cm^{-1} for ALA does not appear in the spectrum of ALA_{inter}–Mt(Na). Instead, a weak and broad band near 3259 cm^{-1} is observed, which is assigned to the symmetric N–H stretching of the $-NH_3^+$ groups. This newly formed band further confirms the protonation of ALA and its intercalation via cation exchange. For pure ALA, two intense bands near 1514 and 1396 cm^{-1} are attributed to the antisymmetric and symmetric stretching of R-COO^-, respectively. As can be seen in Fig. 2c, these bands are absent, and a new band at 1716 cm^{-1} appears

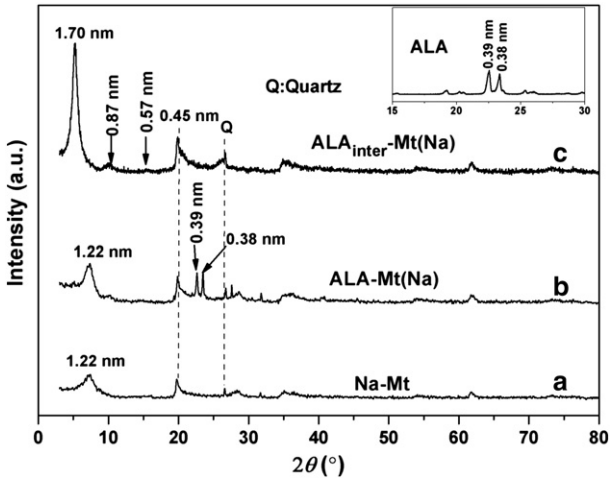

Fig. 1. The XRD patterns of ALA, Na-Mt, and Mt–ALA complexes.

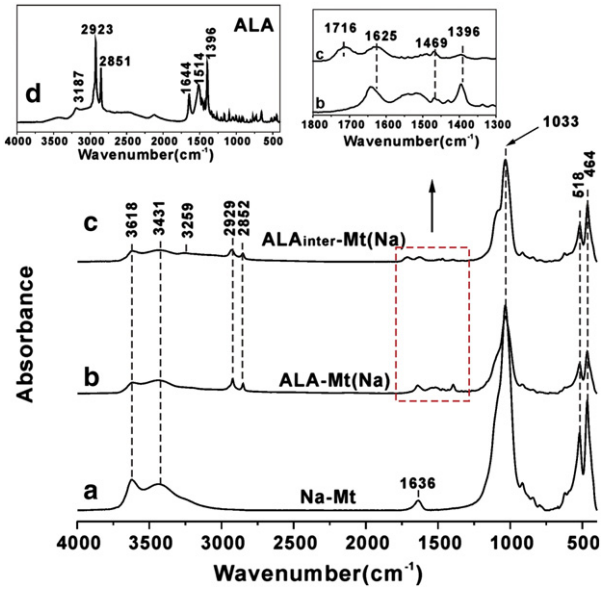

Fig. 2. The FTIR spectra of Na-Mt, ALA, and Mt–ALA complexes.

in the ALA_{inter}–Mt(Na) spectrum, which is attributed to the C═O stretching vibration in nonionized carboxyl groups. During the preparation of ALA_{inter}–Mt(Na), the COO^- groups reverted to COOH when ALA was added to the aqueous solution of HCl and formed a C═O band in the interlayer Mt–ALA complex (Katti et al., 2006). In addition, the vibration of the interlayer water of Na-Mt at 1636 cm^{-1} shifts to 1625 cm^{-1} in ALA_{inter}–Mt(Na). The lower intensity of this band compared with Na-Mt implies the replacement of hydrated sodium cations in ALA_{inter}–Mt(Na) by the protonated ALA.

3.2. Thermal decomposition of pure ALA and Mt–ALA complexes

3.2.1. Thermogravimetric analysis

Fig. 3 displays the TG curves, the corresponding derivative curves (DTG), and the total infrared absorbance profiles (Gram–Schmidt curves) for the Na-Mt, pure ALA, and Mt–ALA complexes as a function of temperature. Na-Mt exhibits two degradation steps. The first step occurs below 200 °C, with a sharp DTG peak at 114 °C. The mass loss in this stage is approximately 12.64%, which is attributed to the elimination of surface-absorbed water (free water) and interlayer water. The second step in the temperature range of 500 to 700 °C corresponds to the dehydroxylation of the clay sheets (He et al., 2005; Xie et al., 2001), in which a broad DTG peak is resolved at 628 °C. Pure ALA started

Table 1
Band assignments of the FTIR spectra of Na-Mt, ALA, and Mt–ALA complexes (Katti et al., 2006; Sikdar et al., 2008).

Wavenumber (cm^{-1})	Bands
3618	O–H stretching of the structural hydroxyl group of Mt
3431	O–H stretching of the water of Mt
3259	NH_3^+ stretching
3187	N–H stretching
2929/2923	CH_2 antisymmetric stretching
2852	CH_2 symmetric stretching
1716	C═O stretching
1644/1625	Combination of O–H deformation and N–H bending
1636	O–H deformation of the water of Mt
1514	R-COO^- antisymmetric stretching
1469	CO–H bending
1396	R-COO^- symmetric stretching
1033	Si–O–Si stretching of Mt
518	Si–O–Al deformation of Mt
464	Si–O–Si bending of Mt

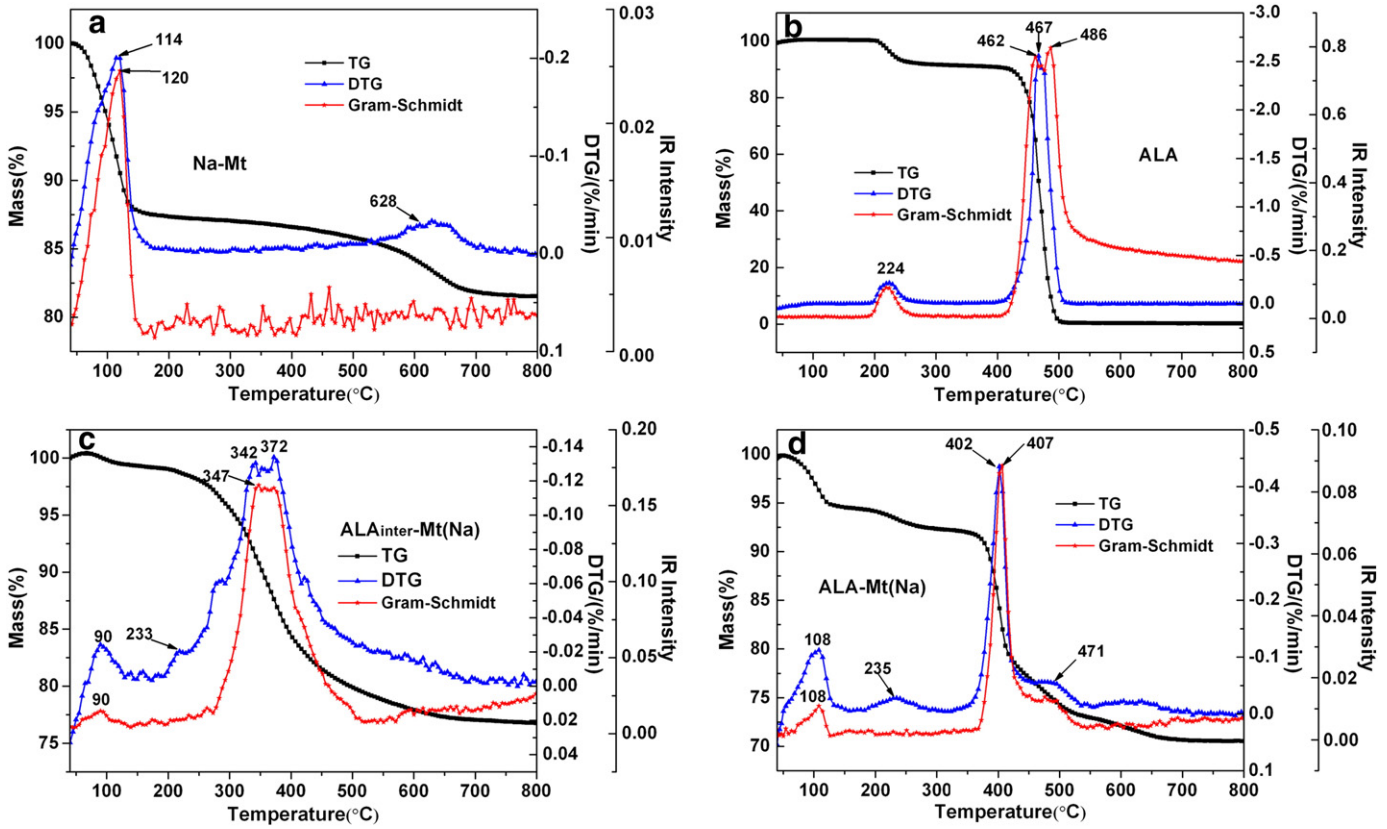

Fig. 3. The TG, DTG, and Gram–Schmidt curves of Na-Mt, ALA, and Mt–ALA complexes.

to decompose above 200 °C, with a small DTG peak at 224 °C (Fig. 3b). The major thermal event of pure ALA occurred in the range of 400 to 550 °C and resulted in a sharp DTG peak at 467 °C.

The TG curve of interlayer Mt–ALA complex in the stage of dehydration (below 200 °C) is much milder than that of Na-Mt (Fig. 3c). The mass loss associated with the water content is only 0.96% for ALA_{inter}–Mt(Na) compared with 12.64% for the Na-Mt, implying the replacement of hydrated sodium cations by ALA. Due to the fact that the residual free water is easily removed at a lower temperature, the DTG peak in this range of ALA_{inter}–Mt(Na) shifts (from 114 °C for Na-Mt) to 90 °C. The mass loss of the interlayer ALA–Mt complex is approximately 19.17% in the temperature range of 200 to 500 °C. As described above, the initial content of ALA in ALA_{inter}–Mt(Na) is 19%. These data indicated that the most of the organic matter within the interlayer space is evolved. Two overlapping peaks of the degradation of organic matter can be observed at 342 and 372 °C for the interlayer Mt–ALA complex, which are significantly lower than the corresponding temperature for pure ALA (approximately 120 °C).

As shown in Fig. 3d, ALA–Mt(Na), the simply mixed sample, exhibits thermal degradation characteristics that are a combination of those of pure ALA and Na-Mt. The release of the absorbed water and interlayer water of Na-Mt occurred below 200 °C. The mass loss is approximately 5.87% at this stage, with a DTG peak at 108 °C. The bulk of ALA in ALA–Mt(Na) evolved rapidly within the temperature range of 350 to 450 °C, in which a sharp DTG peak is resolved at 402 °C. The small DTG peaks at 235 and 471 °C are attributed to a small amount of ALA that was unaffected by the clay minerals and decomposed spontaneously. For the Mt–ALA complexes, the dehydroxylation of Na-Mt is negligible compared with the significant mass loss due to ALA decomposition.

The Gram–Schmidt curves and peaks for all samples match well with the corresponding DTG data (Fig. 3). The slightly higher temperatures of the Gram–Schmidt peaks than those of the DTG peaks indicate the existence of a delay between the gas generation and its detection using the FTIR equipment due to the retained effect of the interlayer space of Na-Mt on the release of evolved gases. The broadness of the range of temperatures corresponding to organic matter decomposition in the TG, DTG, and Gram–Schmidt curves for ALA_{inter}–Mt(Na) can also be attributed to the barrier effect of the clay layers.

Many studies on organoclays showed that the intercalation of surfactant into the interlayer space of clay minerals resulted in an increase in the thermal stability of the surfactant (He et al., 2005; Vazquez et al., 2008; Xi et al., 2007). However, the presence of Na-Mt induces a lower decomposition temperature of ALA in this study, and the lowest temperature is observed in the case of ALA_{inter}–Mt(Na). This result indicates that Na-Mt has a catalytic effect on the decomposition of ALA. Moreover, the interlayer space is an important reaction region, in which the thermal decomposition of ALA is further promoted. The inherent solid acidity of clay minerals enables the clay to act as an efficient solid acid catalyst in organic reactions (Bergaya et al., 2006; Reddy et al., 2007; Singh et al., 2007). As indicated by the measurement of solid acidity, the amounts of total, Brønsted, and Lewis acid sites of Na-Mt are 0.30, 0.09, and 0.21 mmol/g, respectively It is accepted that Lewis acid sites arise from octahedral-coordinated Al^{3+} and/or Fe^{3+} ions exposed at the edges of Mt crystallites. The main source of Brønsted acid sites of Mt is the hydrated cations in the interlayer space. The hydrated cations give rise to Brønsted acidity by polarizing the interlayer water molecules and promoting their dissociation to donate protons.

3.2.2. Evolved gas analysis

The 3D FTIR spectrum of the evolved gases of Na-Mt shows no important bands, except for the intensity signals associated with water (1300–2000 cm^{-1} and 3500–4000 cm^{-1}) at 114 °C (Fig. 4a) (Marini et al., 2003). Fig. 4b shows the 3D FTIR spectrum resulting from the thermal decomposition of pure ALA, and Fig. 5 shows the FTIR spectrum of the evolved gases at the maximum evolution rate (486 °C). Only the characteristic absorbance of water with a low intensity is observed at

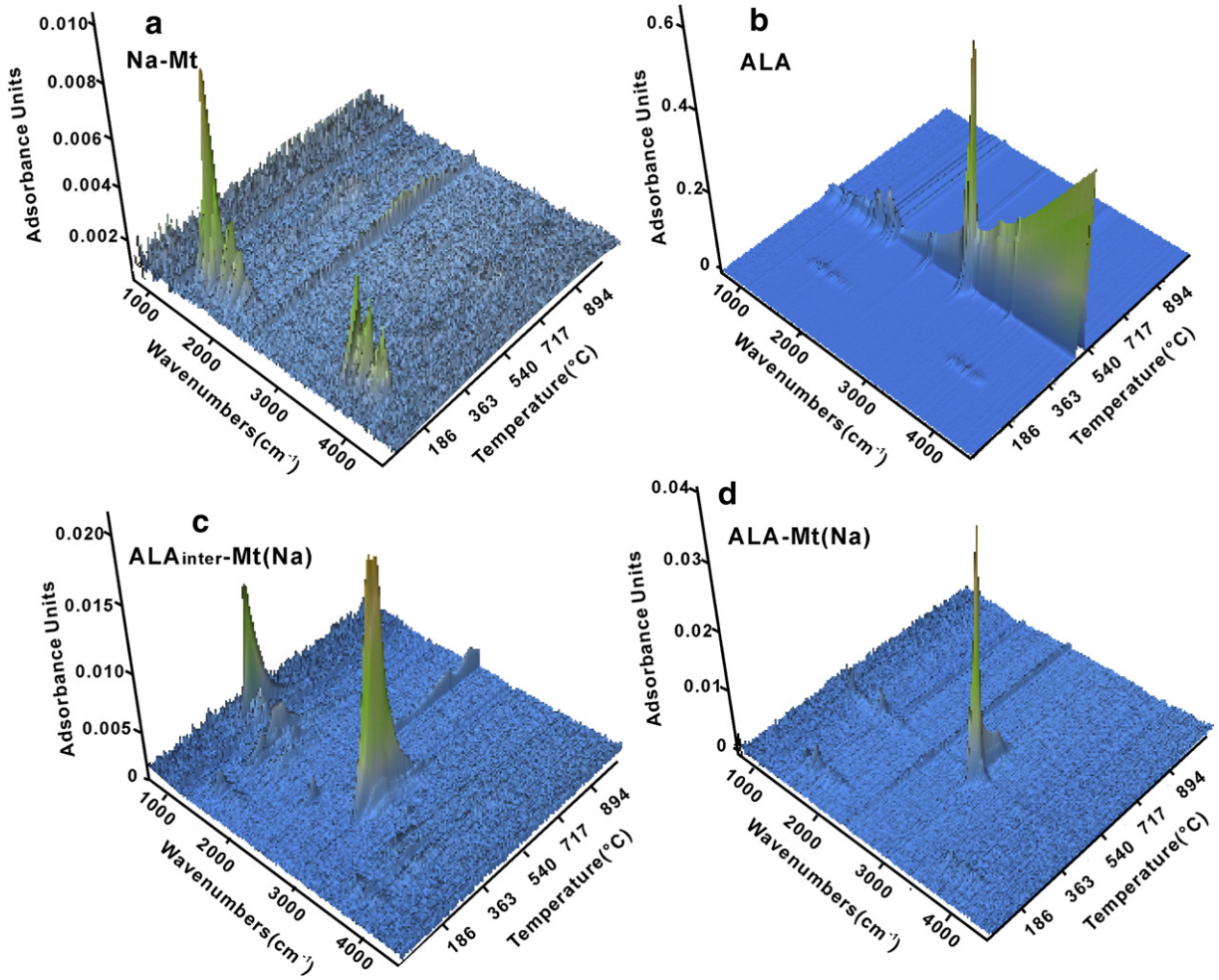

Fig. 4. The 3D-FTIR spectra of the evolved gaseous products of samples.

224 °C from the 3D FTIR spectrum. This result indicates that the small mass loss of pure ALA within the temperature range of 200 to 300 °C is attributed to the release of trace amounts of water. Intermolecular condensation reactions of amino acids occur readily and form water as a product (Li et al., 2008). Because ALA is similar in terms of structure and functional groups to an amino acid, it is reasonable to consider the detected water to be the product of the condensation reaction of ALA. The spectrum obtained at 486 °C exhibits strong bands at 2930 and 2858 cm^{-1}, that are related to the antisymmetrical and symmetrical stretching of methylene groups (Marcilla et al., 2005), respectively, which indicates that the major gaseous products at this stage are aliphatic hydrocarbon fragments. The existence of these groups is confirmed by the presence of bands at 1459 and 1364 cm^{-1}. The band at 1502 cm^{-1} is also related to the –CH bending of hydrocarbons (Zhu et al., 2008). Minor products, such as N-containing compounds (3336 cm^{-1}) and carboxylic acid (3578 and 1777 cm^{-1}) (Pitkänen et al., 1999) are also identified. The detected function group at 1668 cm^{-1} was identified as a carbonyl group in the literature (Liu et al., 2010). This band may originate from carboxylic acid or other carbonyl compounds. The presence of the low-intensity bands at 3086 and 912 cm^{-1} indicates the possible existence of trace amounts of alkene (Huang and Wang, 2009).

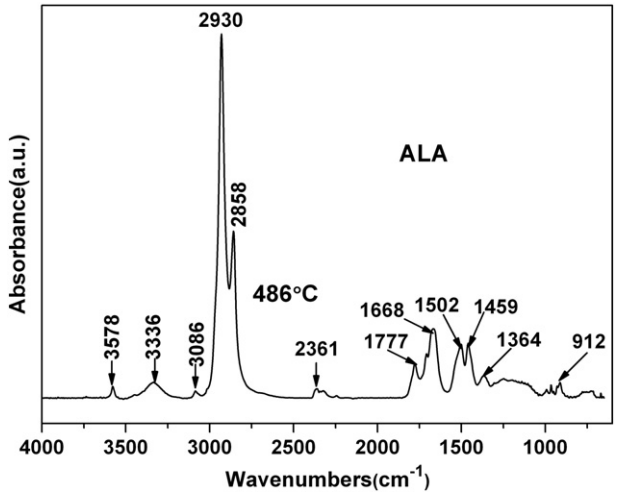

Fig. 5. The FTIR spectrum of the evolved gases from ALA obtained at 486 °C.

The 3D FTIR spectrum of evolved gases of ALA_{inter}–Mt(Na) and the characteristic spectra obtained at 90, 268, 347, and 382 °C are shown in Figs. 4c and 6, respectively. Different thermal decomposition behaviors can clearly be observed between ALA within the interlayer space of Na-Mt and pure ALA. From Figs. 4c and 6, the characteristic bands for water, CO_2 (2359 and 2323 cm^{-1}), aliphatic hydrocarbon (2966–2876 cm^{-1}, 1460 cm^{-1}, and 1382 cm^{-1}), and NH_3 (1625, 966, and 929 cm^{-1}) can be easily identified (Li et al., 2008; Wang et al., 2009). The characteristic bands at 3736, 2359, 2937, and 965 cm^{-1} were chosen to represent water, CO_2, hydrocarbons, and NH_3, respectively, to study the distribution of gaseous products with the increase of

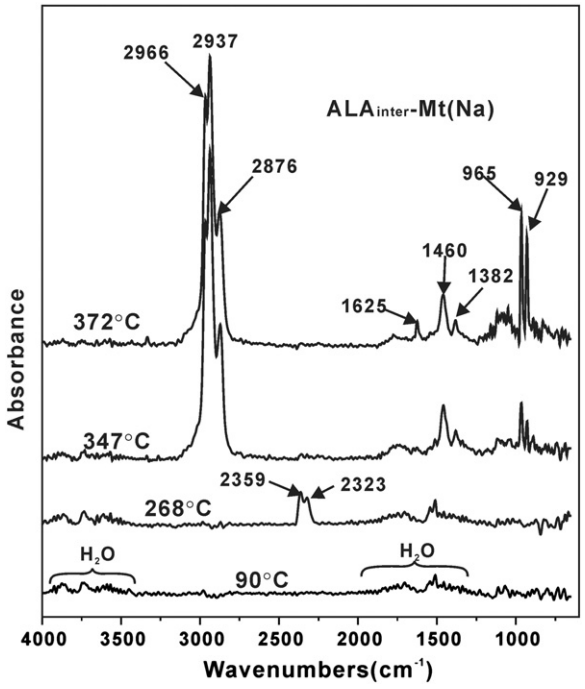

Fig. 6. The FTIR spectra of evolved gases from ALA_{inter}–Mt(Na) obtained at 90, 268, 347, and 372 °C.

temperature. Water is the only gaseous product with a low yield at the beginning of the thermal decomposition (below 100 °C), which corresponds to the first small peak in the Gram–Schmidt curve (Fig. 7a and b). In the temperature range of 200 to 300 °C, the signals of water and CO_2 can be detected (Fig. 7b and c), indicating that ALA underwent dehydration and decarboxylation reactions. Considerable amounts of aliphatic hydrocarbons and NH_3 are formed at temperatures ranging from 270 to 500 °C (Fig. 7d). The maximum release rates of hydrocarbons and NH_3 are reached at 347 and 372 °C, respectively. Therefore, the primary reactions involved in the decomposition process of ALA_{inter}–Mt(Na) are carbon–carbon bond scission and deamination. At higher temperatures, the characteristic bands of hydrocarbon and ammonia disappears, whereas the 3D FTIR spectrum and Fig. 7c show the new formation of the CO_2. This result indicates that a small quantity of carbonaceous residue survived due to the protection of the interlayer space of Mt against heating. In the temperature range of 600 to 800 °C, this residue may react with the oxygen in the crystal structure of the dehydroxylated montmorillonite to yield CO_2. A similar mechanism was proposed for the thermal degradation of alkylammonium-modified montmorillonite (Xie et al., 2001).

The observation of characteristic bands for water at 108 °C in the 3D FTIR spectrum (Fig. 4d) for ALA–Mt(Na) further confirms that the mass loss below 200 °C is attributed to the release of water. Aliphatic hydrocarbon is the main product and exhibits strong bands at 2936, 2867, and 1457 cm^{-1} accompanied by the formation of a small quantity of NH_3 (Fig. 8). Trace amounts of alkene, CH_4, and compounds containing a carboxyl group may also exist due to the appearance of weak bands at 3088, 3018, and 1779 cm^{-1}, respectively (Braun et al., 2007).

The information obtained from TG-FTIR study suggests that Na-Mt not only accelerates the thermal decomposition of ALA but also changes the pathway and products of the decomposition of organics. The decomposition process of pure ALA can be divided into two steps. In the first step, an intermolecular condensation reaction occurred between 200 and 300 °C producing a small quantity of water. In the second step (400 to 550 °C), the cleavage of C – C bonds was the main decomposition reaction of pure ALA, which resulted in the formation of a large amount of aliphatic hydrocarbon and small amounts of carboxylic acid and nitrogen-containing compounds.

Deamination was the main reaction involved in the decomposition process of ALA_{inter}–Mt(Na) and did not occur during the decomposition of ALA alone. The identified evolved gaseous products of ALA_{inter}–Mt(Na) indicate the occurrence of Hoffmann elimination. Xie

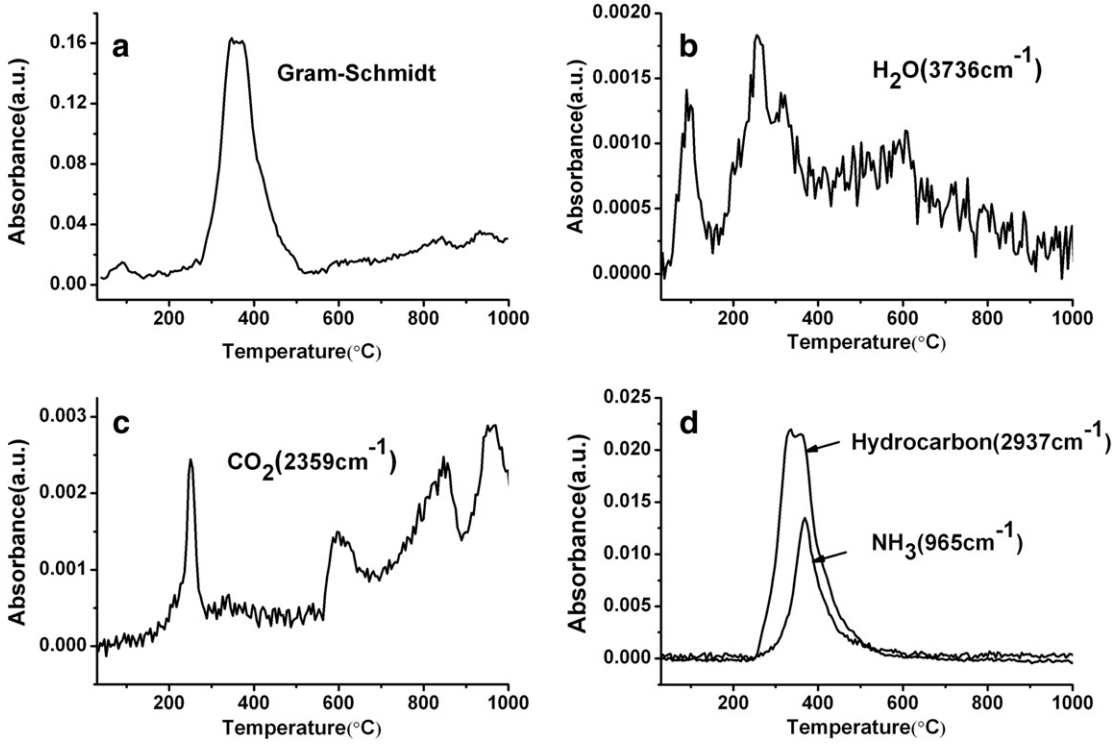

Fig. 7. The distributions of all gaseous products of ALAinter–Mt(Na) with respect to temperature.

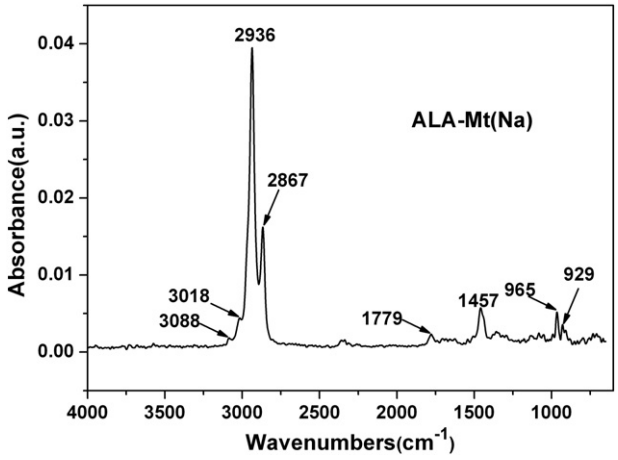

Fig. 8. The FTIR spectrum of evolved gases from ALA–Mt(Na) at 407 °C.

et al. (2001) and Bellucci et al. (2007) reported that alkylammonium-modified montmorillonite was likely to undergo Hoffmann elimination during the heating process, resulting in the formation of ammonia and the corresponding alkene. The generation of NH_3 during the thermal degradation of ALA_{inter}–Mt(Na) can be attributed to two reasons. When ALA was protonated, the formation of $-NH_3^+$ would weaken the C – N bond by increasing the effective electronegativity of the nitrogen (Xie et al., 2001). Moreover, Brønsted acid sites also promote the breakage of the C – N bond, which was supported by the study of Rajagopal et al (1992). Their investigation on the relevance of denitrogenation and solid acidity of SiO_2 suggested that the deamination reaction is strongly dependent on the Brønsted acid sites via the Hofmann elimination pathway. An additional TG-FTIR experiment was performed to evaluate the effect of protonation on the thermal degradation of ALA. The obtained result shows that protonation treatment did not change the decomposition temperature and products of ALA (the detail data were provided in Fig. S1, Fig. S2, and Fig. S3 in Supplementary materials), in the applied experimental condition. That means the Brønsted acid sites in Mt is the predominant reason for the deamination of ALA. The original organic matter in ALA–Mt(Na) was pure ALA. It is interesting to note that the FTIR spectrum of the residue of thermally treated ALA–Mt(Na) (after heating at 200 °C) exhibits the characteristic band of $-NH_3^+$, accompanied by the disappearance of the corresponding band of $-NH_2$ (data not shown). This result indicates that Na-Mt provided protons during the heating process to promote the protonation of the $-NH_2$ group of the ALA. The most probable source of the protons is the dissociation of interlayer water by Na^+, namely Brønsted acid sites. As a result, a small quantity of NH_3 is identified from the gas products of ALA–Mt(Na). According to the definition of Hoffman elimination, alkene is one of the major products. However, no characteristic bands of unsaturated alkyl products are observed in the FTIR spectrum of ALA_{inter}–Mt(Na). A reaction mechanism involving Brønsted acid sites is proposed to account for this observation. Brønsted acid sites in clay minerals can catalyze the hydrogenation reaction and hydrocarbon cracking via the carbonium ion mechanism, which has been supported by several studies (Adams et al., 1983; Galwey, 1970). The elemental analysis shows an incomplete replacement of Na^+ ions by protonated ALA in ALA_{inter}–Mt(Na). The FTIR and TG results show that most of the interlayer water was removed. Mortland and Raman observed that when the water content in the interlayer space decreased, the polarization force of hydrated cations became more concentrated in the remaining water, which increased the proton-donating abilities of this water (Mortland and Raman, 1968). As a result, despite the small quantity of residual hydrated Na^+ cations, the Brønsted acid sites readily provide protons to promote the hydrocracking of unsaturated hydrocarbons to produce lighter saturated products.

In our previous study, pyrolysis experiments were conducted on the ALA and Mt–ALA complexes in a confined gold capsule system at a fixed temperature (350 °C) and pressure (36 MPa) for 48 h (Yuan et al., 2013). The gaseous product analysis showed that Mt promoted the decarboxylation of ALA to yield a considerable amount of CO_2. However, this process did not occur in the current study. The CO_2 that evolved from the Mt–ALA complexes has a noticeable lower absorbance when compared with pure ALA. This inconsistency is attributed to the different experimental systems used. The sealed gold capsule and a longer time in the pyrolysis experiment system increased the ability of Mt to contact and react with ALA. The Lewis acid sites at the edge of Mt can capture an electron from ALA to form a radical intermediate. Through rearrangement, the radical intermediate then forms an alkyl radical and CO_2 (Almon and Johns, 1975). In this study, the entire decomposition process was completed in an open system within an hour, which was not conducive for the Lewis acid sites to promote the decarboxylation of ALA.

3.3. Implications for the transformation of organics in sediment

Nitrogen-containing organics are ubiquitous in surface sediment. They mainly occur in the forms of amido- and amine structures, such as amino acids and proteins. In an acidic microenvironment that is comparable to that applied in this study, it is quite possible that the amido- and amine groups in sediment are protonated and hence intercalated into the interlayer space of clay minerals via cation exchange to form interlayer clay–organic complexes. As summarized by M. Baxby, the total organic nitrogen concentration decreased with the increasing sediment depth and with the increased release of NH_3; the loss of nitrogen was related to biodegradation in the surface sediment and to chemical reactions in the deep stratum (Baxby et al., 1994). Most of the organics within the interlayer space of clay minerals can avoid the biodegradation. The present results obtained from the thermal decomposition of Mt–ALA complexes are consistent with these observations in deep stratum, which demonstrates the significant effect of clay minerals on the thermal transformation of nitrogen-containing organics. The current work demonstrates that clay minerals are capable of catalyzing the denitrogenation of long straight-chain, nitrogen-containing organics to form unsaturated hydrocarbons, and promote the subsequent hydrocracking of these intermediate products. This work further proves that the interlayer space of clay minerals is an important site for the storage and preservation of organic matters and is a significant catalysis region for the related organic reactions. Similar to nitrogen-containing organics, other cationic organics in sediment can also enter into the interlayer space of clay minerals and decompose via the catalysis of solid acid sites. Therefore, the contribution of organic matter within the interlayer space of clay minerals to hydrocarbon generation deserves more attention.

4. Conclusion

The thermal degradation behavior of ALA in the presence of Mt was investigated using TG-FTIR. Pure ALA decomposes via the cleavage of C – C bonds to produce aliphatic hydrocarbons, N-containing compounds, and carboxylic acid. In contrast, ALA in the interlayer Mt–ALA complex undergoes Hoffmann elimination and hydrocracking during the heating process and produces considerable amounts of NH_3 and saturated hydrocarbons. ALA in the mixed Mt–ALA complex shows a similar deamination reaction to that of interlayer Mt–ALA complex but with a lower yield of NH_3. These two reactions are catalyzed by the Brønsted acid sites derived from the dissociation of the interlayer water of Mt. Brønsted acid sites provide protons for the protonation of ALA and induce the cleavage of C – N bonds for deamination. Brønsted acid sites also promote the hydrocracking of unsaturated hydrocarbons to generate saturated hydrocarbons via the carbonium ion mechanism.

These results demonstrate that the solid acidity of Mt plays a significant role in promoting the thermal decomposition of organic matter associated with Mt. The interlayer space of Mt is particularly important because it hosts the cationic organics and provides acid catalytic sites for the degradation of organics. This study indicates that the role of the interlayer space of clay minerals in the hydrocarbon generation deserves more attention in future studies.

Acknowledgments

This work was financially supported by the National Basic Research Program of China (grant no. 2012CB214704-01), the National Natural Science Foundation of China (grant no. 41272059), and the National S&T Major Project of China (grant no. 2011ZX05008-002-21). This is a contribution (no. IS-1675) from GIGCAS.

Appendix A. Supplementary data

Supplementary data to this article can be found online at http://dx.doi.org/10.1016/j.clay.2013.07.005.

References

Adams, J., Clapp, T., Clement, D., 1983. Catalysis by montmorillonites. Clay Minerals 18 (4), 411–421.
Aizenshtat, Z., Miloslavsky, I., Heller-Kallai, L., 1984. The effect of montmorillonite on the thermal decomposition of fatty acids under "bulk flow" conditions. Organic Geochemistry 7 (1), 85–90.
Almon, W.R., Johns, W.D., 1975. Petroleum forming reactions: the mechanism and rate of clay catalyzed fatty acid decarboxylation. Proc. 7th Int. Meet. Org. Geochem. Madrid.
Baxby, M., Patience, R., Bartle, K., 1994. The origin and diagenesis of sedimentary organic nitrogen. Journal of Petroleum Geology 17 (2), 211–230.
Bayrak, Y., 2006. Application of Langmuir isotherm to saturated fatty acid adsorption. Microporous and Mesoporous Materials 87 (3), 203–206.
Bellucci, F., Camino, G., Frache, A., Sarra, A., 2007. Catalytic charring–volatilization competition in organoclay nanocomposites. Polymer Degradation and Stability 92 (3), 425–436.
Bergaya, F., Theng, B.K.G., Lagaly, G., 2006. Handbook of Clay Science, vol. 1. Elsevier Science.
Braun, U., Schartel, B., Fichera, M.A., Jäger, C., 2007. Flame retardancy mechanisms of aluminium phosphinate in combination with melamine polyphosphate and zinc borate in glass-fibre reinforced polyamide 6,6. Polymer Degradation and Stability 92 (8), 1528–1545.
Cai, J., Bao, Y., Yang, S., Wang, X., Fan, D., Xu, J., Wang, A., 2007. Research on preservation and enrichment mechanisms of organic matter in muddy sediment and mudstone. Science in China Series D: Earth Sciences 50 (5), 765–775.
Catrinescu, C., Fernandes, C., Castilho, P., Breen, C., 2006. Influence of exchange cations on the catalytic conversion of limonene over Serra de Dentro (SD) and SAz-1 clays: correlations between acidity and catalytic activity/selectivity. Applied Catalysis A: General 311, 172–184.
Cervantes-Uc, J.M., Espinosa, J.I.M., Cauich-Rodríguez, J.V., Ávila-Ortega, A., Vázquez-Torres, H., Marcos-Fernández, A., San Román, J., 2009. TGA/FTIR studies of segmented aliphatic polyurethanes and their nanocomposites prepared with commercial montmorillonites. Polymer Degradation and Stability 94 (10), 1666–1677.
Cosultchi, A., Bosch, P., Lara, V.H., 2004. Adsorption of petroleum organic compounds on natural Wyoming montmorillonite. Colloids and Surfaces A: Physicochemical and Engineering Aspects 243 (1–3), 53–61.
Drouin, S., Boussafir, M., Robert, J.-L., Alberic, P., Durand, A., 2010. Carboxylic acid sorption on synthetic clays in sea water: in vitro experiments and implications for organo-clay behaviour under marine conditions. Organic Geochemistry 41 (2), 192–199.
Faure, P., Jeanneau, L., Lannuzel, F., 2006. Analysis of organic matter by flash pyrolysis–gas chromatography–mass spectrometry in the presence of Na-smectite: when clay minerals lead to identical molecular signature. Organic Geochemistry 37 (12), 1900–1912.
Galwey, A.K., 1970. Reactions of alcohols and of hydrocarbons on montmorillonite surfaces. Journal of Catalysis 19 (3), 330–342.
Geatches, D.L., Clark, S.J., Greenwell, H.C., 2010. Role of clay minerals in oil-forming reactions. The Journal of Physical Chemistry. A 114 (10), 3569–3575.
Giuntoli, J., de Jong, W., Arvelakis, S., Spliethoff, H., Verkooijen, A.H.M., 2009. Quantitative and kinetic TG-FTIR study of biomass residue pyrolysis: dry distiller's grains with solubles (DDGS) and chicken manure. Journal of Analytical and Applied Pyrolysis 85 (1–2), 301–312.
He, H., Ding, Z., Zhu, J., Yuan, P., Xi, Y., Yang, D., Frost, R.L., 2005. Thermal characterization of surfactant-modified montmorillonites. Clays and Clay Minerals 53 (3), 287–293.
Heller-Kallai, L., Aizenshtat, Z., Miloslavski, I., 1984. The effect of various clay minerals on the thermal decomposition of stearic acid under "bulk flow" conditions. Clay Minerals 19 (5), 779–788.
Huang, N., Wang, J., 2009. A TGA-FTIR study on the effect of $CaCO_3$ on the thermal degradation of EBA copolymer. Journal of Analytical and Applied Pyrolysis 84 (2), 124–130.
Johns, W., 1979. Clay mineral catalysis and petroleum generation. Annual Review of Earth and Planetary Sciences 7 (1), 183–198.
Jurg, J., Eisma, E., 1964. Petroleum hydrocarbons: generation from fatty acid. Science 144 (3625), 1451.
Katti, K.S., Sikdar, D., Katti, D.R., Ghosh, P., Verma, D., 2006. Molecular interactions in intercalated organically modified clay and clay–polycaprolactam nanocomposites: experiments and modeling. Polymer 47 (1), 403–414.
Kennedy, M.J., Pevear, D.R., Hill, R.J., 2002. Mineral surface control of organic carbon in black shale. Science 295 (5555), 657–660.
Lagaly, G., Ogawa, M., Dékány, I., 2006. Clay mineral organic interactions. In: Faïza Bergaya, B.K.G.T., Gerhard, L. (Eds.), Handbook of Clay Science. Elsevier, pp. 309–377.
Li, J., Liu, Y., Shi, J., Wang, Z., Hu, L., Yang, X., Wang, C., 2008. The investigation of thermal decomposition pathways of phenylalanine and tyrosine by TG-FTIR. Thermochimica Acta 467 (1–2), 20–29.
Liu, X., Khor, S., Petinakis, E., Yu, L., Simon, G., Dean, K., Bateman, S., 2010. Effects of hydrophilic fillers on the thermal degradation of poly(lactic acid). Thermochimica Acta 509 (1–2), 147–151.
Liu, D., Yuan, P., Liu, H., Cai, J., Qin, Z., Tan, D., Zhou, Q., He, H., Zhu, J., 2011. Influence of heating on the solid acidity of montmorillonite: a combined study by DRIFT and Hammett indicators. Applied Clay Science 52 (4), 358–363.
Lu, X.C., Hu, W.X., Fu, Q., Miao, D.Y., Zhou, G.J., Hong, Z.H., 1999. Study of combination pattern of soluble organic matters and clay minerals in the immature source rocks in Dongying depression, China. Chinese Journal of Geology 34 (1), 69–77.
Ma, C.-C.M., Kuo, C.-T., Kuan, H.-C., Chiang, C.-L., 2003. Effects of swelling agents on the crystallization behavior and mechanical properties of polyamide 6/clay nanocomposites. Journal of Applied Polymer Science 88 (7), 1686–1693.
Mango, F.D., 2000. The origin of light hydrocarbons. Geochimica et Cosmochimica Acta 64 (7), 1265–1277.
Marcilla, A., Gómez, A., Menargues, S., 2005. TGA/FTIR study of the catalytic pyrolysis of ethylene–vinyl acetate copolymers in the presence of MCM-41. Polymer Degradation and Stability 89 (1), 145–152.
Marini, A., Berbenni, V., Bruni, G., Maggioni, A., Cofrancesco, P., Sinistri, C., Orlandi, A., Villa, M., 2003. Solid-state characterization of a novel chemotherapeutic drug. Journal of Pharmaceutical Sciences 92 (3), 577–584.
Mortland, M., Raman, K., 1968. Surface acidity of smectites in relation to hydration, exchangeable cation, and structure. Clays and Clay Minerals 16 (5), 393–398.
Pan, C., Jiang, L., Liu, J., Zhang, S., Zhu, G., 2010. The effects of calcite and montmorillonite on oil cracking in confined pyrolysis experiments. Organic Geochemistry 41 (7), 611–626.
Pitkänen, I., Huttunen, J., Halttunen, H., Vesterinen, R., 1999. Evolved gas analysis of some solid fuels by TG-FTIR. Journal of Thermal Analysis and Calorimetry 56 (3), 1253–1259.
Rajagopal, S., Grimm, T.L., Collins, D.J., Miranda, R., 1992. Denitrogenation of piperidine on alumina, silica, and silica-aluminas: the effect of surface acidity. Journal of Catalysis 137 (2), 453–461.
Reddy, C.R., Nagendrappa, G., Jai Prakash, B.S., 2007. Surface acidity study of Mn^{+}-montmorillonite clay catalysts by FT-IR spectroscopy: correlation with esterification activity. Catalysis Communications 8 (3), 241–246.
Reichert, P., Kressler, J., Thomann, R., Müllhaupt, R., Stöppelmann, G., 1998. Nanocomposites based on a synthetic layer silicate and polyamide-12. Acta Polymerica 49 (2–3), 116–123.
Shi, J., Xiang, M., Qu, D., Zhou, Y., 1995. Significance of amino acids and fatty acids for the formation of the bio-thermocatalytic transition zone gases. Acta Sedimentologica Sinica 2.
Shimoyama, A., Johns, W.D., 1971. Catalytic conversion of fatty acids to petroleum-like paraffins and their maturation. Nature 232 (33), 140–144.
Sikdar, D., Katti, K.S., Katti, D.R., 2008. Molecular interactions alter clay and polymer structure in polymer clay nanocomposites. Journal of Nanoscience and Nanotechnology 8 (4), 1638–1657.
Singh, B., Patial, J., Sharma, P., Agarwal, S.G., Qazi, G.N., Maity, S., 2007. Influence of acidity of montmorillonite and modified montmorillonite clay minerals for the conversion of longifolene to isolongifolene. Journal of Molecular Catalysis A: Chemical 266 (1–2), 215–220.
Tannenbaum, E., Kaplan, I.R., 1985. Role of minerals in the thermal alteration of organic matter—I: generation of gases and condensates under dry condition. Geochimica et Cosmochimica Acta 49 (12), 2589–2604.
Theng, B.K.G. (Ed.), 1974. The Chemistry of Clay–organic Reactions. Adam Hilger, London.
Theng, B.K.G., Churchman, G.J., Newman, R.H., 1986. The occurrence of interlayer clay–organic complexes in two New Zealand soils. Soil Science 142 (5), 262–266.
Vazquez, A., López, M., Kortaberria, G., Martín, L., Mondragon, I., 2008. Modification of montmorillonite with cationic surfactants. Thermal and chemical analysis including CEC determination. Applied Clay Science 41 (1–2), 24–36.
Wang, M.C., Huang, P.M., 1986. Humic macromolecule Interlayering in nontronite through interaction with phenol monomers. Nature 323 (6088), 529–531.
Wang, Z., Lv, P., Hu, Y., Hu, K., 2009. Thermal degradation study of intumescent flame retardants by TG and FTIR: melamine phosphate and its mixture with pentaerythritol. Journal of Analytical and Applied Pyrolysis 86 (1), 207–214.
Wattel-Koekkoek, E.J.W., van Genuchten, P.P.L., Buurman, P., van Lagen, B., 2001. Amount and composition of clay-associated soil organic matter in a range of kaolinitic and smectitic soils. Geoderma 99 (1–2), 27–49.
Wei, Z., Michael Moldowan, J., Dahl, J., Goldstein, T.P., Jarvie, D.M., 2006. The catalytic effects of minerals on the formation of diamondoids from kerogen macromolecules. Organic Geochemistry 37 (11), 1421–1436.
Xi, Y., Frost, R.L., He, H., 2007. Modification of the surfaces of Wyoming montmorillonite by the cationic surfactants alkyl trimethyl, dialkyl dimethyl, and trialkyl methyl ammonium bromides. Journal of Colloid and Interface Science 305 (1), 150–158.

Xie, W., Gao, Z., Pan, W.-P., Hunter, D., Singh, A., Vaia, R., 2001. Thermal degradation chemistry of alkyl quaternary ammonium montmorillonite. Chemistry of Materials 13 (9), 2979–2990.

Yuan, P., Liu, H., Liu, D., Tan, D., Yan, W., He, H., 2013. Role of the interlayer space of montmorillonite in hydrocarbon generation: an experimental study based on high temperature–pressure pyrolysis. Applied Clay Science 75, 82–91.

Zhang, Z.L., Liu, H.P., Li, B., Ji, Z.K., Lei, N., 2008. Reaction of fatty acid ester catalyzed by minerals at low temperature in heavy water and water. Journal of China University of Petroleum: Edition of Natural Science 32 (5).

Zhu, H.M., Yan, J.H., Jiang, X.G., Lai, Y.E., Cen, K.F., 2008. Study on pyrolysis of typical medical waste materials by using TG-FTIR analysis. Journal of Hazardous Materials 153 (1–2), 670–676.